

## ARTICLE OPEN



# Observing the quantum Cheshire cat effect with noninvasive weak measurement

Yosep Kim<sup>1</sup>, Dong-Gil Im<sup>1</sup>, Yong-Su Kim<sup>2,3</sup>, Sang-Wook Han<sup>2,3</sup>, Sung Moon<sup>2,3</sup>, Yoon-Ho Kim<sup>1</sup> and Young-Wook Cho<sup>2</sup>

One of the common conceptions of nature, typically derived from the experiences with classical systems, is that attributes of the matter coexist with the substance. In the quantum regime, however, the quantum particle itself and its physical property may be in spatial separation, known as the quantum Cheshire cat effect. While there have been several reports to date on the observation of the quantum Cheshire cat effect, all such experiments are based on first-order interferometry and destructive projection measurement, thus allowing simple interpretation due to measurement-induced disturbance and also subject to trivial interpretation based on classical waves. In this work, we report an experimental observation of the quantum Cheshire cat effect with noninvasive weak quantum measurement as originally proposed. The use of the weak-measurement probe has allowed us to identify the location of the single photon and that of the disembodied polarization state in a quantum interferometer. The weak-measurement probe based on two-photon interference makes our observation unable to be explained by classical physics. We furthermore elucidate the quantum Cheshire cat effect as quantum interference of the transition amplitudes for the photon and the polarization state which are directly obtained from the measurement outcomes or the weak values. Our work not only reveals the true quantum nature of Cheshire cat effect but also sheds light on a comprehensive understanding for the counter-intuitive quantum phenomena.

*npj Quantum Information* (2021)7:13; <https://doi.org/10.1038/s41534-020-00350-6>

## INTRODUCTION

Everyday experiences, typically derived from observing classical systems, shape up our common conceptions of nature. Quantum effects, on the other hand, often reveal peculiar counter-intuitive phenomena. One particular example is that the quantum particle itself and its physical property can be spatially separated in the quantum regime. This paradoxical effect is known as the quantum Cheshire cat effect, which was named after a fictional cat appeared in the novel *Alice's Adventures in Wonderland*<sup>1</sup>. The disembodiment of the physical property (i.e., the state) from the particle itself is not only conceptually interesting, but may also provide a way to suppress local decoherence on a certain physical state<sup>2</sup>.

In the literature, the quantum Cheshire cat effect was reported via a neutron experiment<sup>3</sup> and a single-photon experiment<sup>4</sup>, both based on essentially identical Mach-Zehnder interferometry setup shown in Fig. 1. An absorber (ABS) or a half-wave plate (HWP) inserted in one of the interferometric paths *a* or *b* acts as the probe for the particle itself or the disembodied physical state (i.e., spin or polarization). An argument in support of the quantum Cheshire cat effect was made by observing the change of detection rate induced by the probe. For instance, if the photon travels along path *a* (and its polarization state in path *b*), an ABS inserted in path *b* would not affect the detection probability at all. While these early experiments do provide some insights on the quantum Cheshire cat effect phenomenologically, they are based on simple first-order interferometry and destructive projection measurement<sup>3,4</sup>.

The paradoxical observation, i.e. the particle is observed in path *a* and the physical property is found in path *b*, does not hold if the observations are not made on the same ensemble.

The rigorous observation of the quantum Cheshire cat effect, thus, requires the ability to probe simultaneously both the particle itself and the disembodied physical state without disturbing the quantum states<sup>1</sup>. On this basis, only noninvasive weak quantum measurements<sup>5,6</sup> and associated weak values<sup>7–12</sup> allow us to probe the quantum Cheshire cat effect properly. However, the quantum Cheshire cat experiments reported to date are all prone to interpretation based on measurement-induced disturbance and also subject to trivial interpretation based on classical waves. The associated weak values were not directly obtained with noninvasive weak measurement, but inferred from the change of detection rate based on the first-order interference effect. In fact, it is simple to reproduce the Mach-Zehnder type quantum Cheshire cat experiment by using classical light waves, thus requiring no quantum interpretation at all<sup>13,14</sup>. Consequently, it has been argued whether the quantum Cheshire cat effect is a quantum phenomenon<sup>15–19</sup>.

In this work, we report the experimental observation of the quantum Cheshire cat effect with noninvasive weak quantum measurement as originally proposed<sup>1</sup>. The location of the single photon and that of the disembodied polarization state in a quantum interferometer have been identified. Notably, our weak measurement interaction has been implemented based on two-photon interference<sup>20–22</sup>, so that the observation cannot be explained by classical physics. We furthermore elucidate the paradox of the quantum Cheshire cat effect as quantum interference of the transition amplitudes for the photon and the polarization state which are directly obtained from the measurement outcomes or the weak values<sup>16</sup>.

<sup>1</sup>Department of Physics, Pohang University of Science and Technology (POSTECH), Pohang 37673, Korea. <sup>2</sup>Center for Quantum Information, Korea Institute of Science and Technology (KIST), Seoul 02792, Korea. <sup>3</sup>Division of Nano and Information Technology, KIST School, Korea University of Science and Technology, Seoul 02792, Korea. ✉email: yoonho72@gmail.com; choyoungwook81@gmail.com

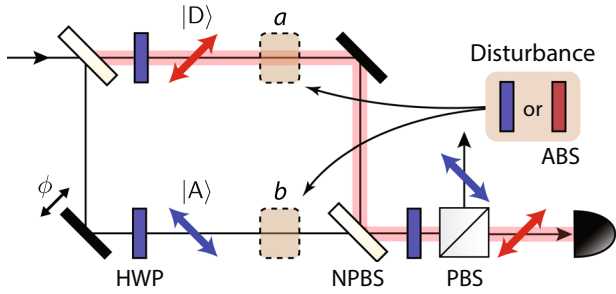


**Fig. 1 Essential schematic based on the Mach-Zehnder interferometer.** A polarized beam is split into two paths with a non-polarizing beam splitter (NPBS). With half-wave plates (HWP), the polarizations in the upper and lower paths, respectively, are set at  $|D\rangle$  and  $|A\rangle$ . The polarizing beam splitter (PBS) ensures that only the  $|D\rangle$  polarization reaches the detector. To probe the locations of the photon itself and its polarization state, an absorber (ABS) or an HWP is inserted in paths  $a$  or  $b$ .

## RESULTS

### Schematic and theory

We illustrate the experimental schematic to observe the quantum Cheshire cat effect in Fig. 2a. The system photon represents the Cheshire cat and its horizontal  $|H\rangle$  and vertical  $|V\rangle$  polarization states correspond to the status of her grin. The disembodiment of the grin (the polarization state) from the cat (the single photon) occurs as the system photon propagates between beam displacers (BD). The initial state of the photon in Fig. 2a after the first BD and HWP is<sup>23</sup>

$$|\Psi_i\rangle_s = \frac{1}{\sqrt{2}}(|u\rangle \otimes |D\rangle + |l\rangle \otimes |A\rangle), \quad (1)$$

where  $|u\rangle$  and  $|l\rangle$  denote the upper and lower paths, respectively, and the polarization states are given as  $|D\rangle = (|H\rangle + |V\rangle)/\sqrt{2}$  and  $|A\rangle = (|H\rangle - |V\rangle)/\sqrt{2}$ . To probe the presence of the photon and its disembodied polarization state at the lower path, the pointer photon, initialized in  $|\Phi_i\rangle_p = |H\rangle$ , is weakly coupled to the system photon for noninvasive measurement. Then, the system photon is subject to projection measurement in the basis,

$$|\Psi_f\rangle_s = \frac{1}{\sqrt{2}}(|u\rangle + |l\rangle) \otimes |D\rangle, \quad (2)$$

and the state of the pointer photon is measured with a quarter-wave plate (QWP), an HWP, and a polarizing beam splitter (PBS).

As shown in Fig. 2a, the system photon in the lower path  $|l\rangle$  is weakly probed for the observable  $\hat{\Pi}_a = |a\rangle\langle a|$  via the measurement interaction of  $\hat{U}_M$ <sup>20,21</sup>. The measurement interaction imparts a rotating operation  $\hat{R}(g/2)$  on the pointer state, conditioned on the system photon's polarization state  $|a\rangle$ , i.e.,  $\hat{U}_M = (\hat{I} - \hat{\Pi}_a) \otimes \hat{I} + \hat{\Pi}_a \otimes \hat{R}(g/2)$ . Here, the rotating operation is defined by  $\hat{R}(\theta)|H\rangle \rightarrow \cos 2\theta|H\rangle + \sin 2\theta|V\rangle$  and  $\hat{R}(\theta)|V\rangle \rightarrow \sin 2\theta|H\rangle - \cos 2\theta|V\rangle$ . A change in the pointer state, induced by the interaction, signifies that the system state is measured by the observable  $\hat{\Pi}_a$ , and the degree of change  $g$  indicates the measurement strength.

The quantum circuit for the unitary interaction  $\hat{U}_M$  is shown in Fig. 2b and its quantum optical implementation is shown in Fig. 2c. The controlled-Z (CZ) gate imposes a  $\pi$ -phase shift on the vertical polarization of the pointer photon only when the system polarization is vertical. The CZ gate is implemented via two-photon quantum interference at a partial PBS having polarization-dependent transmissions ( $T_H = 1$ ,  $T_V = 1/3$ ) with HWP set at  $45^\circ$ <sup>22,24</sup>. The rotating gates are constructed by other HWP. The angles of  $\theta_a$  and  $\theta_g$  determine the observable  $\hat{\Pi}_a$  and the

measurement strength  $g = 4\theta_g$ , respectively. For instance, the observable is given as  $|V\rangle\langle V|$  for  $\theta_a = 0$  and  $|H\rangle\langle H|$  for  $\theta_a = \pi/4$ . Further details on the experimental setup can be found in the "Methods" section.

The total unitary operation acting on the three-mode system-pointer state  $|\Psi_i\rangle_s \otimes |\Phi_i\rangle_p$  is given by<sup>7</sup>

$$\begin{aligned} \hat{U}_{\text{tot}} &= \hat{\Pi}_u \otimes \hat{I} \otimes \hat{I} + \hat{\Pi}_l \otimes \hat{U}_M \\ &= (\hat{I} \otimes \hat{I} - \hat{\Pi}_l \otimes \hat{\Pi}_a) \otimes \hat{I} + \hat{\Pi}_l \otimes \hat{\Pi}_a \otimes \hat{R}(g/2). \end{aligned} \quad (3)$$

For  $g = \pi/2$ , the projection operators on the system state,  $\hat{I} \otimes \hat{I} - \hat{\Pi}_l \otimes \hat{\Pi}_a$  and  $\hat{\Pi}_l \otimes \hat{\Pi}_a$ , are perfectly distinguished by the pointer state and the outcome of the projection measurement can be extracted by analyzing the state of the pointer. In contrast, for  $|g| \ll 1$ , the state of the system photon is weakly coupled to the pointer state, realizing the noninvasive weak measurement which is essential for the observation of the quantum Cheshire cat effect.

In the limit of weak measurement,  $|g| \ll 1$ , the system-pointer evolution is approximated to be

$$\hat{U}_{\text{tot}}|\Psi_i\rangle_s|\Phi_i\rangle_p \approx |\Psi_i\rangle_s|\Phi_i\rangle_p + g\hat{\Pi}_l \otimes \hat{\Pi}_a|\Psi_i\rangle_s|V\rangle_p. \quad (4)$$

Note that the state of the system photon is negligibly disturbed. The post-selection of the system photon onto the final state  $|\Psi_f\rangle_s$  makes the pointer state into

$$|\Phi_f\rangle_p \propto |H\rangle_p + g\langle \hat{\Pi}_l \otimes \hat{\Pi}_a \rangle_w |V\rangle_p, \quad (5)$$

where  $\langle \hat{O} \rangle_w$  indicates the weak value, defined as<sup>7–12</sup>

$$\langle \hat{O} \rangle_w = \frac{\langle \Psi_f | \hat{O} | \Psi_i \rangle}{\langle \Psi_f | \Psi_i \rangle}. \quad (6)$$

The weak value is extracted by analyzing the final pointer state in Eq. (5) as follows:

$$\begin{aligned} \langle \hat{\sigma}_x \rangle_p^a &= 2g \text{Re}(\langle \hat{\Pi}_l \otimes \hat{\Pi}_a \rangle_w), \\ \langle \hat{\sigma}_y \rangle_p^a &= 2g \text{Im}(\langle \hat{\Pi}_l \otimes \hat{\Pi}_a \rangle_w), \end{aligned} \quad (7)$$

where  $\hat{\sigma}_x$  and  $\hat{\sigma}_y$  are Pauli operators and the expectation values are defined as  $\langle \hat{\sigma}_k \rangle_p^a = {}_p\langle \Phi_f | \hat{\sigma}_k | \Phi_f \rangle_p / {}_p\langle \Phi_f | \Phi_f \rangle_p$ . Here, the superscript  $a$  is introduced to denote the observable setting of  $\hat{\Pi}_a$ . The real and imaginary parts, respectively, are associated with the information pertaining to the observable  $\hat{\Pi}_l \otimes \hat{\Pi}_a$  and the measurement back-action induced by the measurement interaction<sup>25–28</sup>.

### Experimental results

For the quantum Cheshire cat effect, the relevant observables are  $\hat{\Pi}_l \otimes \hat{I}$  and  $\hat{\Pi}_l \otimes \hat{\sigma}_z$ , which represent the existence of the system photon itself and the presence of the photon's polarization state in the lower path  $|l\rangle$ , respectively. The measurement outcomes  $\langle \hat{\Pi}_l \otimes \hat{I} \rangle_w = 0$  and  $\langle \hat{\Pi}_l \otimes \hat{\sigma}_z \rangle_w = 1$  represent the observation of the quantum Cheshire cat effect: the polarization state is found in the path in which the system photon does not exist. Although this observation is sufficient to reveal the quantum Cheshire cat effect<sup>1</sup>, i.e. the disembodiment effect, complementary observation is also available by probing the upper path. That is the existence of the photon in the upper path without the polarization, i.e.  $\langle \hat{\Pi}_u \otimes \hat{I} \rangle_w = 1$  and  $\langle \hat{\Pi}_u \otimes \hat{\sigma}_z \rangle_w = 0$ . Alternatively, one may infer the existence of the photon in the upper path from the measurements in the lower path. This counterfactual reasoning is permitted since weak noninvasive measurements allow to probe both paths on the same ensemble due to the negligible disturbance. This feature also coincides in the mathematical sum rule for weak values  $\langle \hat{\Pi}_u \otimes \hat{I} \rangle_w + \langle \hat{\Pi}_l \otimes \hat{I} \rangle_w = 1$ , by which the existence of the photon in the upper path can be inferred. Thus the quantum Cheshire cat effect can be conclusively revealed by measurements for the lower path if the weak noninvasive measurements are properly implemented.

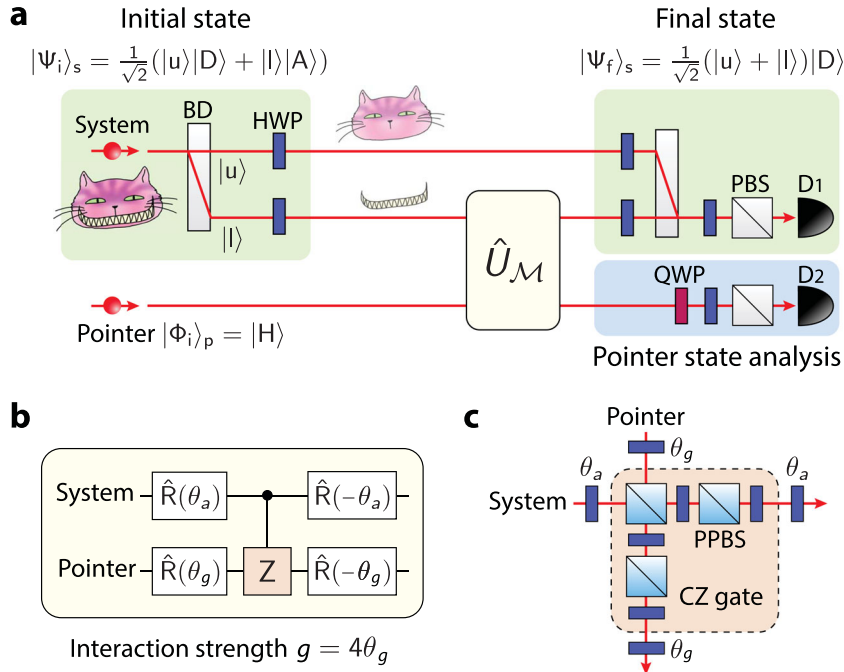


**Fig. 2 Experimental schematic.** **a** The system photon and its polarization are disembodied during the transit through the optical paths. The initial and final states are prepared as presented in the figure using half-wave plates (HWP), beam displacers (BD), and a polarizing beam splitter (PBS). To probe the presence of the photon and the disembodied polarization state at the lower path, the system photon is weakly coupled to the pointer photon via the unitary interaction  $\hat{U}_M$ . The quantum circuit for the unitary interaction is shown in **b** and its quantum optical implementation is shown in **c**. Note that the controlled-Z (CZ) gate is implemented via two-photon quantum interference at a partial polarizing beam splitter (PPBS) having polarization-dependent transmissions ( $T_H = 1$ ,  $T_V = 1/3$ ) with HWP set at  $45^\circ$ . The pointer state is finally measured with a quarter-wave plate (QWP), an HWP, and a PBS.

We would like to make it clear that the paradoxical observation is valid only if the system is weakly measured. The strong projective measurement cannot even observe the paradoxical effect properly; the post-measurement state will be fully collapsed into one of the eigenstates of the measurement observable and, therefore, the sum of the transition probabilities  $|\langle\Psi_f|\hat{\Pi}_I \otimes \hat{\Pi}_H|\Psi_i\rangle|^2 + |\langle\Psi_f|\hat{\Pi}_I \otimes \hat{\Pi}_V|\Psi_i\rangle|^2$  does not exhibit the null transition of a photon in the lower path,  $\langle\hat{\Pi}_I \otimes \hat{\mathbb{I}}\rangle_w = 0$ .

We obtain the weak values of  $\hat{\Pi}_I \otimes \hat{\mathbb{I}}$  and  $\hat{\Pi}_I \otimes \hat{\sigma}_z$  from the linear combinations of the weak values of  $\hat{\Pi}_I \otimes \hat{\Pi}_H$  and  $\hat{\Pi}_I \otimes \hat{\Pi}_V$  by making use of the relations  $\hat{\mathbb{I}} = \hat{\Pi}_H + \hat{\Pi}_V$  and  $\hat{\sigma}_z = \hat{\Pi}_H - \hat{\Pi}_V$  as follows:

$$\begin{aligned} \langle\hat{\Pi}_I \otimes \hat{\mathbb{I}}\rangle_w &= \langle\hat{\Pi}_I \otimes \hat{\Pi}_H\rangle_w + \langle\hat{\Pi}_I \otimes \hat{\Pi}_V\rangle_w, \\ \langle\hat{\Pi}_I \otimes \hat{\sigma}_z\rangle_w &= \langle\hat{\Pi}_I \otimes \hat{\Pi}_H\rangle_w - \langle\hat{\Pi}_I \otimes \hat{\Pi}_V\rangle_w. \end{aligned} \quad (8)$$

According to Eq. (7), the real and imaginary parts of  $\langle\hat{\Pi}_I \otimes \hat{\mathbb{I}}\rangle_w$  are obtained from  $(\langle\hat{\sigma}_x\rangle_p^H + \langle\hat{\sigma}_x\rangle_p^V)/2g$  and  $(\langle\hat{\sigma}_y\rangle_p^H + \langle\hat{\sigma}_y\rangle_p^V)/2g$  at  $|g| \ll 1$ , and  $\langle\hat{\Pi}_I \otimes \hat{\sigma}_z\rangle_w$  is estimated similarly.

The experimental confirmation for the observation of the quantum Cheshire cat effect is shown in Fig. 3 in which the pointer measurements  $\langle\hat{\sigma}_x\rangle_p^H + \langle\hat{\sigma}_x\rangle_p^V$  and  $\langle\hat{\sigma}_x\rangle_p^H - \langle\hat{\sigma}_x\rangle_p^V$  are shown as a function of the measurement strength  $g$ . Each measurement interaction for  $\langle\hat{\sigma}_x\rangle_p^H$  and  $\langle\hat{\sigma}_x\rangle_p^V$  is implemented by setting the HWP angle  $\theta_a$  in Fig. 2c as  $45^\circ$  and  $0^\circ$ , respectively. Then, the pointer state, conditioned on the projection measurement of the system onto the state  $|\Psi_f\rangle_s$  at detector D1, is analyzed from the coincident detection events of D1 and D2 with the set of a QWP, an HWP, and a PBS at detector D2. The expectation values of  $\langle\hat{\sigma}_x\rangle_p^H$  and  $\langle\hat{\sigma}_x\rangle_p^V$  are obtained at each  $g$ , and the sum and the difference are given as the data points in Fig. 3a, b for the real parts of  $\langle\hat{\Pi}_I \otimes \hat{\mathbb{I}}\rangle_w$  and  $\langle\hat{\Pi}_I \otimes \hat{\sigma}_z\rangle_w$ , respectively. Note that the imaginary parts have zero value, so the results for  $\langle\hat{\sigma}_y\rangle_p^a$  are not presented.

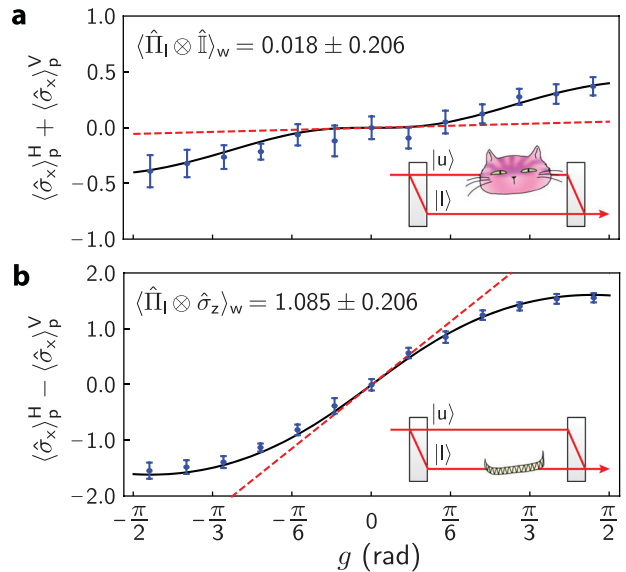


**Fig. 3 Experimental observation of the quantum Cheshire cat effect.** The observation is realized by measuring weak values. Measurements of pointer states (solid circle) are recorded as a function of  $g$  for observables: **a**  $\hat{\Pi}_I \otimes \hat{\mathbb{I}}$  and **b**  $\hat{\Pi}_I \otimes \hat{\sigma}_x$ . Note that the imaginary parts have zero value, so the results for  $\langle\hat{\sigma}_y\rangle_p^a$  are not presented. One standard deviation due to Poissonian counting statistics are considered as error bars. The black solid lines are the exact theoretical predictions. For given observables, weak values are extracted by taking the first-order derivative with polynomial curve fit at  $g=0$ . The measurement results of  $\langle\hat{\Pi}_I \otimes \hat{\mathbb{I}}\rangle_w = 0.018 \pm 0.206$  and  $\langle\hat{\Pi}_I \otimes \hat{\sigma}_z\rangle_w = 1.085 \pm 0.206$  indicate the quantum Cheshire cat effect that the physical property (polarization) can be found in the path where the physical carrier (photon) does not exist.

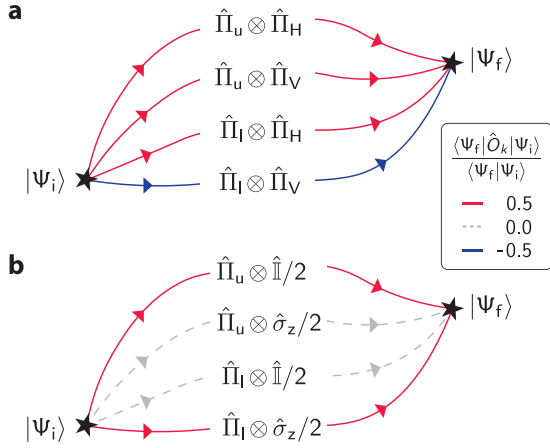


**Fig. 4 Conceptual Feynman diagrams for the transition from  $|\Psi_i\rangle$  to  $|\Psi_f\rangle$ .** The virtual paths defined by  $\hat{O}_k$  can be arbitrarily set to satisfy  $\sum_k \hat{O}_k = \hat{I}$  so that  $\langle \Psi_f | \Psi_i \rangle = \sum_k \langle \Psi_f | \hat{O}_k | \Psi_i \rangle$ . **a**  $\hat{O}_k = \{\hat{\Pi}_u \otimes \hat{\Pi}_H, \hat{\Pi}_u \otimes \hat{\Pi}_V, \hat{\Pi}_l \otimes \hat{\Pi}_H, \hat{\Pi}_l \otimes \hat{\Pi}_V\}$ , **b**  $\hat{O}_k = \{\hat{\Pi}_u \otimes \hat{I}/2, \hat{\Pi}_u \otimes \hat{\sigma}_z/2, \hat{\Pi}_l \otimes \hat{I}/2, \hat{\Pi}_l \otimes \hat{\sigma}_z/2\}$ , where  $\hat{\Pi}_u$  and  $\hat{\Pi}_l$  represent the spatial modes of the state and  $\hat{\Pi}_H$  and  $\hat{\Pi}_V$  represent the polarization modes of the state. The transition amplitudes along the virtual paths in **a** and **b** are related with each other due to  $\hat{I} = \hat{\Pi}_H + \hat{\Pi}_V$  and  $\hat{\sigma}_z = \hat{\Pi}_H - \hat{\Pi}_V$ . The line color shows the normalized transition amplitude of each virtual paths by the total transition amplitude  $\langle \Psi_f | \Psi_i \rangle$  for the initial and final states in Eqs. (1) and (2).

The weak values are extracted from the experimental data in Fig. 3 from the slope at  $g=0$  by using the polynomial fit to the data according to the relation in Eq. (7). The experimentally obtained weak values are  $\langle \hat{\Pi}_l \otimes \hat{I} \rangle_w = 0.018 \pm 0.206$  and  $\langle \hat{\Pi}_l \otimes \hat{\sigma}_z \rangle_w = 1.085 \pm 0.206$  are in good agreement with the theoretical prediction and clearly demonstrate the quantum Cheshire cat effect.

### Quantum interference of transition amplitudes

While the quantum Cheshire cat effect may look paradoxical, we may interpret the effect as quantum interference of the transition amplitudes for the photon and the polarization state. The weak value of Eq. (6), formally, can be interpreted as the transition amplitude  $\langle \Psi_f | \hat{O} | \Psi_i \rangle$  along the virtual path defined by  $\hat{O}$  from the initial state  $|\Psi_i\rangle$  to the post-selected final state  $|\Psi_f\rangle$ , which is normalized by the total transition amplitude  $\langle \Psi_f | \Psi_i \rangle$ <sup>16</sup>. Considering the spatial modes  $\hat{\Pi}_u$  and  $\hat{\Pi}_l$  and the polarization modes  $\hat{\Pi}_H$  and  $\hat{\Pi}_V$ , as the eigenmodes of  $\hat{I}$  and  $\hat{\sigma}_z$ , there are four possible virtual transition paths represented by the following observables, see Fig. 4a.

$$\hat{\Pi}_u \otimes \hat{\Pi}_H, \hat{\Pi}_u \otimes \hat{\Pi}_V, \hat{\Pi}_l \otimes \hat{\Pi}_H, \hat{\Pi}_l \otimes \hat{\Pi}_V, \quad (9)$$

where the observables sum to the identity operator, i.e., they form a complete set. The weak values, namely the normalized transition amplitudes  $\langle \hat{O} \rangle_w = \langle \Psi_f | \hat{O} | \Psi_i \rangle / \langle \Psi_f | \Psi_i \rangle$ , for the initial and final states in Eqs. (1) and (2) are given as

$$\begin{aligned} \langle \hat{\Pi}_u \otimes \hat{\Pi}_H \rangle_w &= 0.5, \quad \langle \hat{\Pi}_u \otimes \hat{\Pi}_V \rangle_w = 0.5, \\ \langle \hat{\Pi}_l \otimes \hat{\Pi}_H \rangle_w &= 0.5, \quad \langle \hat{\Pi}_l \otimes \hat{\Pi}_V \rangle_w = -0.5. \end{aligned} \quad (10)$$

Note that all the normalized transition amplitudes are non-zero and the sum total of the amplitudes is equal to unity.

Similarly, as shown in Fig. 4b, another complete set of virtual transition paths exists as the following observables:

$$\hat{\Pi}_u \otimes \hat{I}/2, \hat{\Pi}_l \otimes \hat{I}/2, \hat{\Pi}_u \otimes \hat{\sigma}_z/2, \hat{\Pi}_l \otimes \hat{\sigma}_z/2, \quad (11)$$

where the observables also sum to the identity operator. The corresponding normalized transition amplitudes for the initial and final states in Eqs. (1) and (2) are calculated as

$$\begin{aligned} \langle \hat{\Pi}_u \otimes \hat{I}/2 \rangle_w &= 0.5, \quad \langle \hat{\Pi}_u \otimes \hat{\sigma}_z/2 \rangle_w = 0, \\ \langle \hat{\Pi}_l \otimes \hat{I}/2 \rangle_w &= 0, \quad \langle \hat{\Pi}_l \otimes \hat{\sigma}_z/2 \rangle_w = 0.5. \end{aligned} \quad (12)$$

The normalized transition amplitudes signify that the system photon can be found in the only upper path  $|u\rangle$  while the polarization appears in the only lower path  $|l\rangle$  during the transition.

The quantum Cheshire cat effect in Eq. (12) can be understood as the interference between the fundamental transition amplitudes in Eq. (10)<sup>16</sup>. The observables in Eq. (11) can be expressed as the linear combination of the observables in Eq. (9), e.g.,  $\hat{\Pi}_l \otimes \hat{I} = \hat{\Pi}_l \otimes \hat{\Pi}_H + \hat{\Pi}_l \otimes \hat{\Pi}_V$  and  $\hat{\Pi}_l \otimes \hat{\sigma}_z = \hat{\Pi}_l \otimes \hat{\Pi}_H - \hat{\Pi}_l \otimes \hat{\Pi}_V$ . Consequently, it is possible to interpret the transition amplitudes in Eq. (12) as the outcomes of constructive and destructive interference between the transition amplitudes in Eq. (10). For instance, the paradoxical null transition amplitude  $\langle \hat{\Pi}_l \otimes \hat{I}/2 \rangle_w$  in Fig. 4b can be resolved as a destructive interference of  $\langle \hat{\Pi}_l \otimes \hat{\Pi}_H \rangle_w$  and  $\langle \hat{\Pi}_l \otimes \hat{\Pi}_V \rangle_w$  having a phase difference of  $\pi$ , as shown in Fig. 4a. The quantum interference can be observed directly by using weak-measurement probes for  $\hat{\Pi}_l \otimes \hat{I}$  and  $\hat{\Pi}_l \otimes \hat{\sigma}_z$ . It is noteworthy that the negative weak value of  $\langle \hat{\Pi}_l \otimes \hat{\Pi}_V \rangle_w$  is anomalous in the sense that it lies outside the eigenvalue spectrum of the projector  $\hat{\Pi}_l \otimes \hat{\Pi}_V$ . The anomalous weak value has been regarded as a quantum signature as they are connected to the quantum contextuality<sup>29–35</sup> and the violation of classical macroscopic realism<sup>36–38</sup>.

### DISCUSSION

The disembodiment of polarization from a photon has been experimentally observed via weak measurements and understood in terms of the transition amplitudes. However, what we conclusively tell from the experimental observations is that the weakly coupled pointer indicates the disembodiment effect. The physical reality of the disembodiment effect must be argued very carefully. The orthodox interpretation to quantum physics represents that the reality of quantum properties is primarily attributed by collapsing the quantum state into an eigenstate through projective measurements<sup>15,16</sup>. If one upholds this view, ascribing the disembodiment effect to the physical reality should not be taken. Nevertheless, it is hard to simply refuse the reality of the disembodiment effect because observation should be associated with the physical reality. If there was no disembodiment, the weak-measurement probes for  $\hat{\Pi}_l \otimes \hat{I}$  and  $\hat{\Pi}_l \otimes \hat{\sigma}_z$  should be affected by the presence of a photon and polarization. However, the null transition amplitudes in Eq. (12) show that the pointer states remain unshifted after the post-selection of  $|\Psi_f\rangle$ . Thus, the null transition amplitudes may be interpreted as the absence of the particle or the physical property<sup>17,39</sup>.

To conclude, we have reported the experimental observation of the quantum Cheshire cat effect, which may provide a way to improve the quality of quantum technologies by suppressing local decoherence<sup>2</sup>. As suggested in the original proposal<sup>1</sup>, we have probed the photon's existence and its polarization property using a noninvasive weak measuring apparatus during the state transition. The noninvasive weak measuring apparatus was realized by coupling the quantum system with the quantum pointer by utilizing another single photon. The weak-measurement interaction based on the two-photon interference made our observation unable to be explained by classical physics<sup>20–22</sup>. The quantum pointer reveals the quantum Cheshire cat effect in the framework of the weak value measurement and the apparent quantum Cheshire cat paradox was explained as quantum interference of virtual transition paths. Our experimental apparatus can be applied to investigate other paradoxical

phenomena based on weak value such as Hardy's paradox<sup>40–42</sup>, Leggett–Garg inequality<sup>37,43,44</sup>, and quantum pigeonhole paradox<sup>45,46</sup> within the proper weak-measurement framework.

Note added. During our manuscript being reviewed, we became aware of a relevant work by Z.-H. Liu et al.<sup>47</sup>, where the second-order quantum interference was involved to reveal the quantum nature of the quantum Cheshire cat effect. While the second-order quantum interference is employed in our experiment for the weak noninvasive system-pointer measurement interaction, the weak values in the experiment by Z.-H. Liu et al. were only inferred from the linear relation between the post-selection probability and the perturbation strength. Instead, in their experiment, the second-order quantum interference appeared for introducing two quantum Cheshire cats, demonstrating the exchange of grins between two cats<sup>47,48</sup>.

## METHODS

### Experimental details

The system and the pointer photons at 780 nm are produced via spontaneous parametric down conversion from a type-II beta-barium borate crystal pumped by a 390 nm pulsed laser. The single photons are delivered to the experimental setup shown in Fig. 2a via the single-mode optical fibers and interfere with each other for the measurement interaction  $U_{M}$ . To ensure high degree of spectral indistinguishability, necessary for high-visibility two-photon quantum interference, 1-nm bandwidth interference filters are placed in front of the detector  $D_1$  and  $D_2$ .

## DATA AVAILABILITY

Data are available from the corresponding authors upon reasonable request.

Received: 24 April 2020; Accepted: 16 November 2020;

Published online: 28 January 2021

## REFERENCES

- Aharonov, Y., Popescu, S., Rohrlich, D. & Skrzypczyk, P. Quantum Cheshire cats. *New J. Phys.* **15**, 113015 (2013).
- Richter, M., Dziewit, B. & Dajka, J. The quantum Cheshire cat effect in the presence of decoherence. *Adv. Math. Phys.* **2018**, 7060586 (2018).
- Denkmayr, T. et al. Observation of a quantum Cheshire cat in a matter-wave interferometer experiment. *Nat. Commun.* **5**, 4492 (2014).
- Ashby, J. M., Schwarz, P. D. & Schlosshauer, M. Observation of the quantum paradox of separation of a single photon from one of its properties. *Phys. Rev. A* **94**, 012102 (2016).
- Banaszek, K. Fidelity balance in quantum operations. *Phys. Rev. Lett.* **86**, 1366–1369 (2001).
- Baek, S.-Y., Cheong, Y. W. & Kim, Y.-H. Minimum-disturbance measurement without postselection. *Phys. Rev. A* **77**, 060308 (R) (2008).
- Kim, Y. et al. Direct quantum process tomography via measuring sequential weak values of incompatible observables. *Nat. Commun.* **9**, 192 (2018).
- Aharonov, Y., Albert, D. Z. & Vaidman, L. How the result of a measurement of a component of the spin of a spin-1/2 particle can turn out to be 100. *Phys. Rev. Lett.* **60**, 1351–1354 (1988).
- Dressel, J., Malik, M., Miatto, F. M., Jordan, A. N. & Boyd, R. W. Colloquium: Understanding quantum weak values: basic and applications. *Rev. Mod. Phys.* **86**, 307–316 (2014).
- Piacentini, F. et al. Measuring incompatible observables by exploiting sequential weak values. *Phys. Rev. Lett.* **117**, 170402 (2016).
- Thekkadath, G. S. et al. Direct measurement of the density matrix of a quantum system. *Phys. Rev. Lett.* **117**, 120401 (2016).
- Cho, Y.-W., Lim, H.-T., Ra, Y.-S. & Kim, Y.-H. Weak value measurement with an incoherent measuring device. *New J. Phys.* **12**, 023036 (2010).
- Atherton, D. P., Ranjit, G., Geraci, A. A. & Weinstein, J. D. Observation of a classical Cheshire cat in an optical interferometer. *Opt. Lett.* **40**, 879–881 (2015).
- Stuckey, W. M., Silberstein, M. & McDevitt, T. Concerning quadratic interaction in the quantum Cheshire cat experiment. *Int. J. Quantum Found.* **2**, 17–31 (2015).
- Corrêa, R., Santos, M. F., Monken, C. H. & Saldanha, P. L. Quantum Cheshire cat' as simple quantum interference. *New J. Phys.* **17**, 053042 (2015).

- Sokolovski, D. Weak measurements measure probability amplitudes (and very little else). *Phys. Lett. A* **380**, 1593–1599 (2016).
- Duprey, Q., Kanjilal, S., Sinha, U., Home, D. & Matzkin, A. The quantum Cheshire cat effect: theoretical basis and observational implications. *Ann. Phys.* **391**, 1–15 (2018).
- Quach, J. Q. Dual to the anomalous weak-value effect of photon-polarization separation. *Phys. Rev. A* **100**, 052117 (2019).
- Michielsen, K., Lippert, T. & Raedt, H. D. Mysterious quantum Cheshire cat: an illusion. *Proc. SPIE* **9570**, 180–185 (2015).
- Pryde, G. J., O'Brien, J. L., White, A. G., Ralph, T. C. & Wiseman, H. M. Measurement of quantum weak values of photon polarization. *Phys. Rev. Lett.* **94**, 220405 (2005).
- Pryde, G. J., O'Brien, J. L., White, A. G., Bartlett, S. D. & Ralph, T. C. Measuring a photonic qubit without destroying it. *Phys. Rev. Lett.* **92**, 190402 (2004).
- Kiesel, N., Schmid, C., Weber, U., Ursin, R. & Weinfurter, H. Linear optics controlled-phase gate made simple. *Phys. Rev. Lett.* **95**, 210505 (2005).
- Kim, Y.-H. Single-photon two-qubit entangled states: preparation and measurement. *Phys. Rev. A* **67**, 040301 (2003).
- Hong, C. K., Ou, Z. Y. & Mandel, L. Measurement of subpicosecond time intervals between two photons by interference. *Phys. Rev. Lett.* **59**, 2044–2046 (1987).
- Cho, Y.-W. et al. Emergence of the geometric phase from quantum measurement back-action. *Nat. Phys.* **15**, 665–670 (2019).
- Jozsa, R. Complex weak values in quantum measurement. *Phys. Rev. A* **76**, 044103 (2007).
- Hofmann, H. F. On the role of complex phases in the quantum statistics of weak measurements. *New J. Phys.* **13**, 103009 (2011).
- Dressel, J. & Jordan, A. N. Significance of the imaginary part of the weak value. *Phys. Rev. A* **85**, 012107 (2012).
- Pusey, M. F. Anomalous weak values are proofs of contextuality. *Phys. Rev. Lett.* **113**, 200401 (2014).
- Qin, L., Feng, W. & Li, X.-Q. Simple understanding of quantum weak values. *Sci. Rep.* **6**, 20286 (2016).
- Piacentini, F. et al. Experiment investigating the connection between weak values and contextuality. *Phys. Rev. Lett.* **116**, 180401 (2016).
- Waegell, M. et al. Confined contextuality in neutron interferometry: observing the quantum pigeonhole effect. *Phys. Rev. A* **96**, 052131 (2017).
- Waegell, M. & Tollaksen, J. Contextuality, pigeonholes, Cheshire cats, mean kings, and weak values. *Quantum Stud.: Math. Found.* **5**, 325–349 (2018).
- Leifer, M. S. & Spekkens, R. W. Pre- and post-selection paradoxes and contextuality in quantum mechanics. *Phys. Rev. Lett.* **95**, 200405 (2005).
- Tollaksen, J. Pre- and post-selection, weak values and contextuality. *J. Phys. A* **40**, 9033–9066 (2007).
- Williams, N. S. & Jordan, A. N. Weak values and the Leggett-Garg inequality in solid-state qubits. *Phys. Rev. Lett.* **100**, 026804 (2008).
- Goggin, M. E. et al. Violation of the Leggett-Garg inequality with weak measurements of photons. *Proc. Natl. Acad. Sci. U.S.A.* **108**, 1256–1261 (2011).
- Dressel, J., Broadbent, C. J., Howell, J. C. & Jordan, A. N. Experimental violation of two-party Leggett-Garg inequalities with semiweak measurements. *Phys. Rev. Lett.* **106**, 040402 (2011).
- Duprey, Q. & Matzkin, A. Null weak values and the past of a quantum particle. *Phys. Rev. A* **95**, 032110 (2017).
- Aharonov, Y., Botero, A., Popescu, S., Reznik, B. & Tollaksen, J. Revisiting Hardy's paradox: counterfactual statements, real measurements, entanglement and weak values. *Phys. Lett. A* **301**, 130–138 (2002).
- Lundeen, J. S. & Steinberg, A. M. Experimental joint weak measurement on a photon pair as a probe of Hardy's paradox. *Phys. Rev. Lett.* **102**, 020404 (2009).
- Yokota, K., Yamamoto, T., Koashi, M. & Imoto, N. Direct observation of Hardy's paradox by joint weak measurement with an entangled photon pair. *New J. Phys.* **11**, 033011 (2009).
- Leggett, A. J. & Garg, A. Quantum mechanics versus macroscopic realism: is the flux there when nobody looks? *Phys. Rev. Lett.* **54**, 857 (1985).
- Palacios-Laloy, A. et al. Experimental violation of a Bell's inequality in time with weak measurement. *Nat. Phys.* **6**, 442–447 (2010).
- Aharonov, Y. et al. Quantum violation of the pigeonhole principle and the nature of quantum correlations. *Proc. Natl. Acad. Sci. U.S.A.* **113**, 532–535 (2016).
- Chen, M.-C. et al. Experimental demonstration of quantum pigeonhole paradox. *Proc. Natl. Acad. Sci. U.S.A.* **116**, 1549–1552 (2019).
- Liu, Z.-H. et al. Experimental exchange of grins between quantum Cheshire cats. *Nat. Commun.* **11**, 3006 (2020).
- Das, D. & Pati, A. K. Can two quantum Cheshire cats exchange grins? *New J. Phys.* **22**, 063032 (2020).

## ACKNOWLEDGEMENTS

This work was supported by the National Research Foundation of Korea (Grant Nos. 2019R1A2C3004812, 2019M3E4A107866011, and 2019M3E4A1079777), the ITRC support program (IITP-2020-0-01606), and the KIST institutional program (Project

No. 2E30620). Y.K. acknowledges support from the Global Ph.D. Fellowship by the National Research Foundation of Korea (Grant No. 2015H1A2A1033028).

### AUTHOR CONTRIBUTIONS

Y.-W.C. and Y.-H.K. planned and supervised the research; Y.K. and Y.-W.C. carried out the experiment and the theoretical calculations; Y.K., Y.-W.C., and Y.-H.K. analyzed the data; D.-G.I., Y.-S.K., S.-W.H., and S.M. contributed the discussion of the results; Y.K., Y.-W.C., and Y.-H.K. wrote the manuscript with input from all authors.

### COMPETING INTERESTS

The authors declare no competing interests.

### ADDITIONAL INFORMATION

**Correspondence** and requests for materials should be addressed to Y.-H.K. or Y.-W.C.

**Reprints and permission information** is available at <http://www.nature.com/reprints>

**Publisher's note** Springer Nature remains neutral with regard to jurisdictional claims in published maps and institutional affiliations.



**Open Access** This article is licensed under a Creative Commons Attribution 4.0 International License, which permits use, sharing, adaptation, distribution and reproduction in any medium or format, as long as you give appropriate credit to the original author(s) and the source, provide a link to the Creative Commons license, and indicate if changes were made. The images or other third party material in this article are included in the article's Creative Commons license, unless indicated otherwise in a credit line to the material. If material is not included in the article's Creative Commons license and your intended use is not permitted by statutory regulation or exceeds the permitted use, you will need to obtain permission directly from the copyright holder. To view a copy of this license, visit <http://creativecommons.org/licenses/by/4.0/>.

© The Author(s) 2021